Separation and Purification Technology 330 (2024) 125299

Contents lists available at ScienceDirect

Separation and Purification Technology

journal homepage: www.elsevier.com/locate/seppur

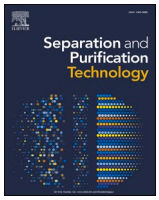

Joint incremental learning network for flexible modeling of carbon dioxide solubility in aqueous mixtures of amines

Yu-Da Hsiao, Chuei-Tin Chang *

Department of Chemical Engineering, National Cheng Kung University, Tainan 701, Taiwan

ARTICLE INFO

Editor: Dr. S Yi

Keywords:
CO_2 solubility
Vapor–liquid equilibrium
Aqueous amine mixtures
Incremental learning
Artificial neural networks

ABSTRACT

Vapor-liquid equilibrium (VLE) modeling is one of the most essential tasks for rigorous estimations of thermodynamic properties in chemical process design and analysis. To realize any commercially feasible carbon dioxide (CO_2) capture scheme using a carefully chosen aqueous amine solution, the accurate model of CO_2 solubility in this water-amine system plays a vital role. However, the experimental data of various mixtures of amine solvents are insufficient and expensive to acquire. In view of this problem, a novel joint incremental learning network (JILN) structure is proposed for modeling equilibrium solubility of CO_2 in various bi-solvent aqueous amine mixtures. With the proposed method, the knowledge embedded in the well-trained mono-solvent models can be extracted and effectively transferred to their related multi-solvent models. By adopting the proposed modeling method, the numerical experimental results showed that the mean absolute percentage errors (MAPEs) for various bi-solvent models were 2.1–4.9%, which indicates a maximum of 68% reduction in prediction blunders if compared with their ANN counterparts.

1. Introduction

To address the pressing issue of global warming, a large number of carbon dioxide (CO_2) capture schemes have been proposed in the past few decades to recover the massive carbon dioxide continuously emitted to the atmosphere by various human activities. For the industrial-scale post-combustion CO_2 capture (PCC) applications, the chemical absorption using amine solutions is considered to be the most mature means to remove CO_2 from the exhaust gas streams. However, the main drawback of this technology is its high energy consumption required for solvent regeneration. As a result, various improvements, i.e., process modifications and absorbent enhancements [1,2], have been proposed to facilitate energy reduction. In particular, numerous experimental studies on investigations of the organic amine solvents have been tried to improve the absorption/regeneration performances by blending various amine solvents [3].

To improve the efficiency of amine scrubbing process via novel and more effective blends, the previous studies obviously strived to identify amine solvents with the characteristics of high CO_2 capture capacity, fast absorption rate and low regeneration energy. In order to rigorously analyze the effects of amine solutions on process systems, the vapor–liquid equilibrium (VLE) behaviors, viscosity, heat and mass transfer properties and reaction kinetic parameters should all be investigated thoroughly. The experiments on equilibrium solubility of CO_2 in many different aqueous amine solutions is considered to be of critical importance since both transport properties and reaction kinetics rely primarily on the VLE behavior [4]. Several VLE models, e.g., Kent-Eisenberg model [5], Deshmukh-Mather model [6], electrolyte-NRTL model [7], and extended UNIQUAC model [8], have already been developed on theoretical basis to predict the thermodynamic properties of the sour gas-amine systems. However, these models are applicable only in narrow applicable temperature and concentration ranges [9].

Machine learning (ML) techniques have frequently been used for assisting the development of PCC technologies [10–12]. Various data-driven modeling techniques, e.g., artificial neural networks (ANNs), are commonly utilized for non-linear regression and classification. These powerful tools have already been applied to process-level modeling, analysis and optimization of PCC simulation studies and pilot plant testing [13–16]. On the other hand, the ANN models were also built to accurately predict the critical physiochemical properties, e.g., density, viscosity, surface tensions, enthalpy and CO_2 equilibrium solubility, of various aqueous amine solutions [17–19]. Also, the equilibrium solubility of CO_2 in aqueous piperazine (PZ) solutions were modeled with ANNs, the adaptive neuro-fuzzy inference system (ANFIS) and the least-

* Corresponding author.
E-mail address: ctchang@mail.ncku.edu.tw (C.-T. Chang).

https://doi.org/10.1016/j.seppur.2023.125299
Received 17 July 2023; Received in revised form 20 September 2023; Accepted 5 October 2023
Available online 8 October 2023

squares support vector machine (LSSVM) models [20,21]. Similarly, the ANN model for CO_2 solubility in aqueous 2-amino-2-methyl-1-propanol (AMP) was constructed and compared with the Deshmukh–Mather model [22]. In addition, other types of ML methods, such as the back-propagation neural network (BPNN), the radial basis function neural network (RBFNN), the general regression neural network (GRNN), the extreme gradient boosting (XGBoost) and the AdaBoost-decision tree (AdaBoost-DT) models, were also adopted to predict the CO_2 solubility in aqueous solutions of various primary, secondary and tertiary amines [4,9,23–26].

Notice that the aforementioned works focused primarily on modeling CO_2 solubility in single amine solutions instead of their blends. Several recent simulation researches and pilot studies showed that it is not only theoretically sound but practically feasible to enhance CO_2 capture efficiencies by blending different amine solvents [27–30]. The unhindered primary and secondary amines possess fast absorption kinetics, while the hindered and tertiary ones may be selected due to their high loading capacities [31]. Therefore, accurate predictions of VLE behaviors of these mixtures seems to be very critical for developing advanced PCC technologies. Several researchers attempted to build semi-empirical models for CO_2 solubility the blended amine solutions by extending the Kent-Eisenberg framework originally applied to the single amine cases [31–33], while some others worked on establishing rigorous kinetic models based on the zwitterion mechanism and the base-catalyzed mechanism for blends of primary, secondary and tertiary amines [34]. A few data-driven models of CO_2 solubility in aqueous blends of alkanolamines or ionic liquids (ILs) have been proposed, while those with alkanolamines have already been constructed by using ANN representations [23,35–38]. For modeling CO_2 solubility in aqueous amine mixtures, the apparent molecular weight was suggested to be selected as an input to characterize the changes in solution composition [36]. In addition to the above CO_2 solubility models, the density, viscosity, surface tension and heat capacity of aqueous amine blends were also carried out in a number of studies by applying the ML tools [39–42]. For mathematically characterizing transport phenomena, some applied generic ML models to predict mass transfer coefficient in packed columns, and it was recently suggested that the acidity dissociation coefficient also plays an important role in predicting the properties of amines [43,44].

It should be noted that the above-mentioned data-driven black-box models are typically system dependent [45], which implies low reusability. If the same approach is followed for property prediction in new solvent systems, the corresponding VLE models have to be built from scratch again. Although such case-by-case regression strategy is nonetheless still feasible in principle, the experimental data of aqueous amine blends may be scarce and, also, it is quite expensive to collect additional data via a large number of experiments. Especially, it should be noted that the above data-acquisition and modeling problems can become even more challenging when new solvents and their blends are under consideration [4,24]. In view of the aforementioned practical difficulties, a novel joint incremental learning network (JILN) was developed in this work to facilitate flexible modeling of CO_2 equilibrium solubility in a wide variety of multi-solvent aqueous amine solutions. With the proposed JILN configuration, the useful prior knowledge embedded in pre-trained VLE models of aqueous mono-amine solutions may be selectively fine-tuned, extracted and reused for joint incremental learning of the VLE models of their blends. This modeling strategy enables effective reuse of the physically meaningful parameters of base models and also greatly enhances the prediction accuracy of the multi-solvent models. In this work, five extensively studied amine solvents, i.e., monoethanolamine (MEA), diethanolamine (DEA), methyldiethanolamine (MDEA), AMP and PZ, and their various bi-solvent aqueous blends were adopted as realistic examples to confirm the general effectiveness of the proposed approach.

2. Relevant background

Although the black-box ML models have already been shown to be superior to their conventional counterparts [9], the domain knowledge extracted from either rigorous or semi-empirical theories is still important for acquiring a deeper understanding of the thermochemical systems and thus facilitating more appropriate designs of ML models. Therefore, a brief review of theoretical background information is given below in this section.

The mechanisms of CO_2 absorption into aqueous amine solutions can be generally divided into the physical and chemical elements. The physical solubility may be characterized by the Henry's law, as shown below in Eq. (1).

$$P_{CO_2} = H_{CO_2}[CO_2] \tag{1}$$

where P_{CO_2} is the partial pressure of CO_2; H_{CO_2} is the Henry's law constant of CO_2, which is temperature dependent; $[CO_2]$ is the concentration of dissolved CO_2 in aqueous solutions.

On the other hand, to be able to adequately describe the chemical solubility of CO_2 in aqueous amines, the rigorous and semi-empirical models have both been widely studied and applied in the last several decades [32,46,47]. Since the key factor dominating the CO_2 loading capacity of primary and secondary amines is the formation of carbamate [31,46], it is crucial to establish its rigorous chemical kinetic theory. For primary and secondary amines, the carbamate formation may be well characterized by the zwitterion mechanism suggested by Danckwerts [48]. The zwitterion mechanism was originally proposed by Caplow as a three-step kinetics [49], which was later simplified into a two-step framework consisting of both the formation and the deprotonation of zwitterion intermediate [46,50]. On the other hand, without free proton, the carbamate is not formed in the cases of tertiary amines. However, based on the base-catalyzed hydration mechanism proposed by Donaldson and Nguyen [51], the tertiary amines, which are weak bases in aqueous solutions, still promote the CO_2 hydration process [4].

Aside from the elaborate kinetic mechanisms mentioned above, for equilibrium solubility modeling, it is common to develop semi-empirical system models that are governed by reversible and mutually independent reactions [4,9,31–33]. More specifically, the aforementioned rigorous transient kinetic mechanisms may be replaced and covered by the apparent equilibrium reactions shown in Table 1 [32,33,52]. All amines undergo water ionization, bicarbonate formation, carbonate formation and amine protonation/deprotonation. On the other hand, as previously mentioned, the carbamate hydrolysis only takes place in aqueous solutions of primary or secondary amines, e.g., MEA, DEA and AMP [31,32]. Notice that PZ, which is a cyclic diamine, goes through two additional carbamate-related reactions, i.e., di-carbamate hydrolysis and carbamate protonation [53,54]. The apparent equilibrium constants for the above reactions can then be described by the Kent-Eisenberg model [32,55]. Both the Henry's law constant (H_{CO_2}) in Eq. (1) and the equilibrium constants (K_i) of the reactions mentioned above in Table 1 are nonlinear functions of temperature, and may be expressed in a general form as:

$$\ln K_i = C_1 + C_2/T + C_3 \ln T + C_4 T \tag{2}$$

where C_1–C_4 are the regression coefficients associated with a particular amine solution. These coefficients and also the Henry's law constant can be found in literatures [56,57].

In addition to the chemical kinetics, three conservation equations, i.e., the amine balance, the carbon balance and the charge balance, should be included to impose both material balance and electro-neutrality of the amine–H_2O–CO_2 system models [9,32]. Notice that carbon balance, amine balance and charge balance equations for different alkanolamines are listed below in Table 2. Theoretically, the CO_2 equilibrium solubility in aqueous amines may be determined by solving the Henry's law in Eq. (1), the Kent-Eisenberg equilibrium constants in Table 1 and the carbon

Table 1
The semi-empirical model based on several apparent equilibrium reactions.

No.	Reactions	Kent-Eisenberg constants	Amines
1	$H_2O \leftrightarrow H^+ + OH^-$	$K_1 = [H^+][OH^-]$	All
2	$CO_2 + H_2O \leftrightarrow H^+ + HCO_3^-$	$K_2 = \frac{[H^+][HCO_3^-]}{[CO_2]}$	All
3	$HCO_3^- \leftrightarrow H^+ + CO_3^{2-}$	$K_3 = \frac{[H^+][CO_3^{2-}]}{[HCO_3^-]}$	All
4	$AmH^+ \leftrightarrow Am + H^+$	$K_4 = \frac{[Am][H^+]}{[AmH^+]}$	All
5	$AmCOO^- + H_2O \leftrightarrow Am + HCO_3^-$	$K_5 = \frac{[Am][HCO_3^-]}{[AmCOO^-]}$	MEA, DEA, AMP
6	$Am(COO^-)_2 + H^+ \leftrightarrow AmCOO^- + CO_2$	$K_6 = \frac{[AmCOO^-][CO_2]}{[Am(COO^-)_2][H^+]}$	PZ
7	$H^+AmCOO^- \leftrightarrow AmCOO^- + H^+$	$K_7 = \frac{[AmCOO^-][H^+]}{[H^+AmCOO^-]}$	PZ

Table 2
The conservative equations for different aqueous amine systems.

No.	Conservation constraints	Amines
Carbon balance equations		
1	$\alpha_{CO_2}[Am]_0 = [CO_2] + [HCO_3^-] + [CO_3^{2-}] + [AmCOO^-]$	MEA, DEA, AMP
2	$\alpha_{CO_2}[Am]_0 = [CO_2] + [HCO_3^-] + [CO_3^{2-}]$	MDEA
3	$\alpha_{CO_2}[Am]_0 = [CO_2] + [HCO_3^-] + [CO_3^{2-}] + [AmCOO^-] + [H^+AmCOO^-] + 2[Am(COO^-)_2]$	PZ
Amine balance equations		
4	$[Am]_0 = [Am] + [AmH^+] + [AmCOO^-]$	MEA, DEA, AMP
5	$[Am]_0 = [Am] + [AmH^+]$	MDEA
6	$[Am]_0 = [Am] + [AmH^+] + [AmCOO^-] + [H^+AmCOO^-] + [Am(COO^-)_2]$	PZ
Charge balance equations		
7	$[H^+] + [AmH^+] = [OH^-] + [HCO_3^-] + 2[CO_3^{2-}] + [AmCOO^-]$	MEA, DEA, AMP
8	$[H^+] + [AmH^+] = [OH^-] + [HCO_3^-] + 2[CO_3^{2-}]$	MDEA
9	$[H^+] + [AmH^+] = [OH^-] + [HCO_3^-] + 2[CO_3^{2-}] + [AmCOO^-] + 2[Am(COO^-)_2]$	PZ

and amine balances in Table 2 simultaneously [9,31,32]. Thus, it can be concluded that the CO_2 equilibrium solubility in aqueous amine solution is closely related to the concentrations of carbon dioxide, alkanolamines and hydrogen ion. Consequently, the CO_2 solubility in aqueous amine can be treated as a function of system temperature, initial concentration of amine and partial pressure of CO_2 [9,25].

3. Neural network models

3.1. Feedforward neural network

Feedforward neural network (FNN), aka multi-layer perceptron (MLP), is one of the most widely used neural network models for engineering applications. A typical fully-connected FNN structure used in this study is shown in Fig. 1, which allows the linear and/or non-linear activation calculations to be performed layer-wisely from input to output layer. The linear transformation is usually applied to the output layer in regression applications, while the non-linear ones, e.g., hyperbolic tangent or rectified linear unit (ReLU), are almost always selected at the hidden layers. The FNN structure can be expressed in a generalized mathematical format as follows:

$$\mathbf{h}_i = \phi(\mathbf{W}_i\mathbf{h}_{i-1} + \mathbf{b}_i) \tag{3}$$

where i is the index of the hidden layers, and $\mathbf{W}_i$ and $\mathbf{b}_i$ are the weight matrix and bias vector in hidden layer i respectively. Clearly, one can see that the above equations are used for linearly transforming hidden-state vector $\mathbf{h}_{i-1}$ from the previous layer $i-1$, and, finally, ϕ in Eq. (3) is the nonlinear activating operator of each entity in any given vector.

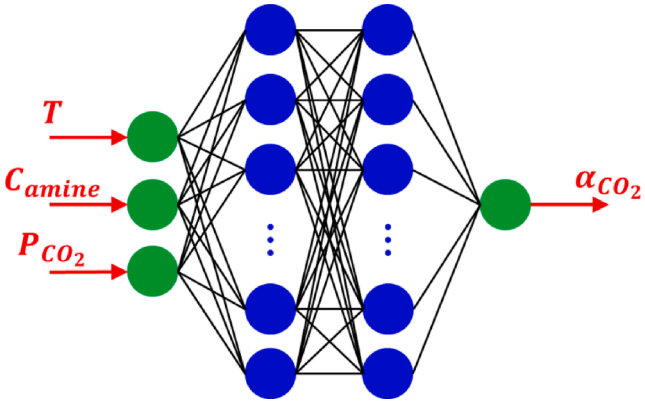

Fig. 1. Feedforward neural network for modeling CO_2 solubility.

3.2. Incremental learning

As a type of connectionist models, the FNN structures are highly flexible that can be configured to form almost infinite number of possible architectures. This special feature naturally leads to the development of ANN block-modularization techniques [58]. With high flexibility, various special network designs, e.g., random vector functional link (RVFL), modular neural network (MNN) and progressive neural network (PNN), have been developed for engineering applications related to transfer and/or incremental learning [59–61].

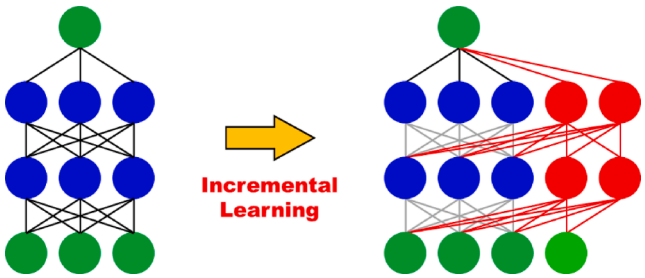

Fig. 2. Incremental learning using feedforward neural network.

Numerous incremental learning (aka continual learning, lifelong learning or progressive learning) techniques have already been developed to effectively preserve and transfer the useful knowledge gained from previous training tasks by freezing, isolating and expanding a subset of designated network parameters (see Fig. 2) in order to ward off catastrophic interferences in model development stages [61–63]. These incremental learning techniques have been applied to process systems engineering (PSE) for mechanistic knowledge transfer and effective enhancement of modeling performance [64,65]. However, to our best knowledge, no published studies tried to explore the applicability of incremental learning for thermodynamic modeling. In addition, the attempts to establish paradigms for complex model building via integration of incremental and joint learning techniques have rarely been made before.

For modeling CO_2 solubility in aqueous amine solutions and mixtures with ANNs, it is theoretically and practically feasible to just train them from scratch in a case-by-case manner. However, since the experimental data is expensive and also hard to come by, this brute-force approach is often impractical or even infeasible. To address these issues, the incremental learning strategies seem to be attractive alternatives to build better models by reusing the weights and biases learnt from the previous training tasks in constructing the simpler models.

4. Model development method

As shown in Fig. 3, the proposed JILN modeling procedure consists of two stages, i.e., model pre-training and joint incremental learning. The base models of mono-solvent systems were constructed first, while the joint incremental learning process were next facilitated by combining these base models. To be more specific, the mono-solvent base models were trained by the dataset obtained from mono-solvent experiments, which are denoted in Fig. 3 as dataset A and dataset B. After building highly accurate and applicable mono-solvent models, denoted as model A and model B in this paper, they may be jointly expanded to accommodate the additional information for amine-blend systems. To solve the problem of distribution shifts among different datasets, a distribution shift model should be pre-trained by both mono-solvent and bi-solvent datasets and then attached to the input layer of the final model. Finally, the dataset obtained from bi-solvent experiments, denoted as dataset A/B, is then used to train the bi-solvent model, i.e., model A/B, in a supervised manner. The training details can be found in the following subsections.

4.1. CO_2 solubility models for single amines

In this study, the multi-layer FNN models introduced in subsection 3.1 were adopted for modeling the CO_2 solubility in any aqueous amine solution. As mentioned in Section 2, both the Henry's law constant and the equilibrium constants in Eq. (2) are nonlinear functions of temperature. On the other hand, the CO_2 solubility may be determined by these constants and the conservative equations in Table 2. Therefore, it may also be concluded that the CO_2 solubility in various aqueous amine solutions are functions of initial amine concentration and partial pressure of CO_2. As a result, the input–output structure of CO_2 solubility models may in general be expressed as [9,25]:

$$\alpha_{CO_2} = f(T, C_{\text{amine}}, P_{CO_2}) \tag{4}$$

where T is the temperature (K) of solution; C_{amine} is the concentration (wt %) of amine; P_{CO_2} is the partial pressure (kPa) of CO_2.

4.2. Distribution shifting layer

Since the parameters of mono-solvent models were completely preserved during the joint incremental learning step, the problem of distribution shift in input variables (i.e., temperature, partial pressure of CO_2 and concentration of amines) in the datasets of different single amine solutions and amine mixtures should be properly resolved to avoid negative transfer [66]. In the current study, this particular problem was overcome by simply passing the new data through a fully-connected layer that performs linear transformations, which may be mathematically expressed as:

$$\mathbf{x}^{(j)} = \mathbf{W}_0^{(j)}\mathbf{x} + \mathbf{b}_0^{(j)} \tag{5}$$

where $\mathbf{x}$ is the input vector of JILN models; $\mathbf{W}_0^{(j)}$, $\mathbf{b}_0^{(j)}$ and $\mathbf{x}^{(j)}$ represent respectively the weight matrix, the bias vector and the input vector connected to each mono-solvent model j.

In practice, the linear layers were end-to-end pre-trained in a self-supervised manner. The testing R^2 scores of these pre-trained layers were all over 0.999 or even approaching 1, which implies that the linear transformations were almost perfect. By adopting the so-called net-to-

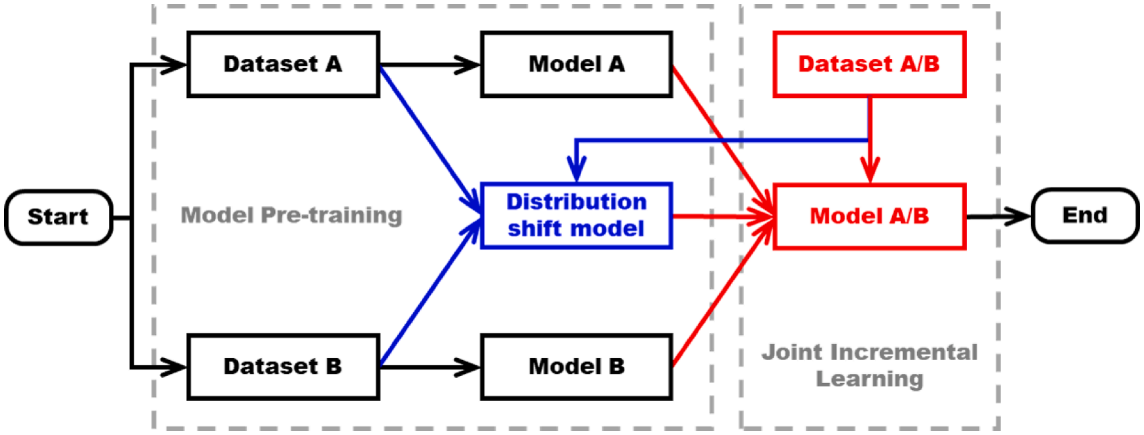

Fig. 3. The proposed modeling procedure for joint incremental learning.

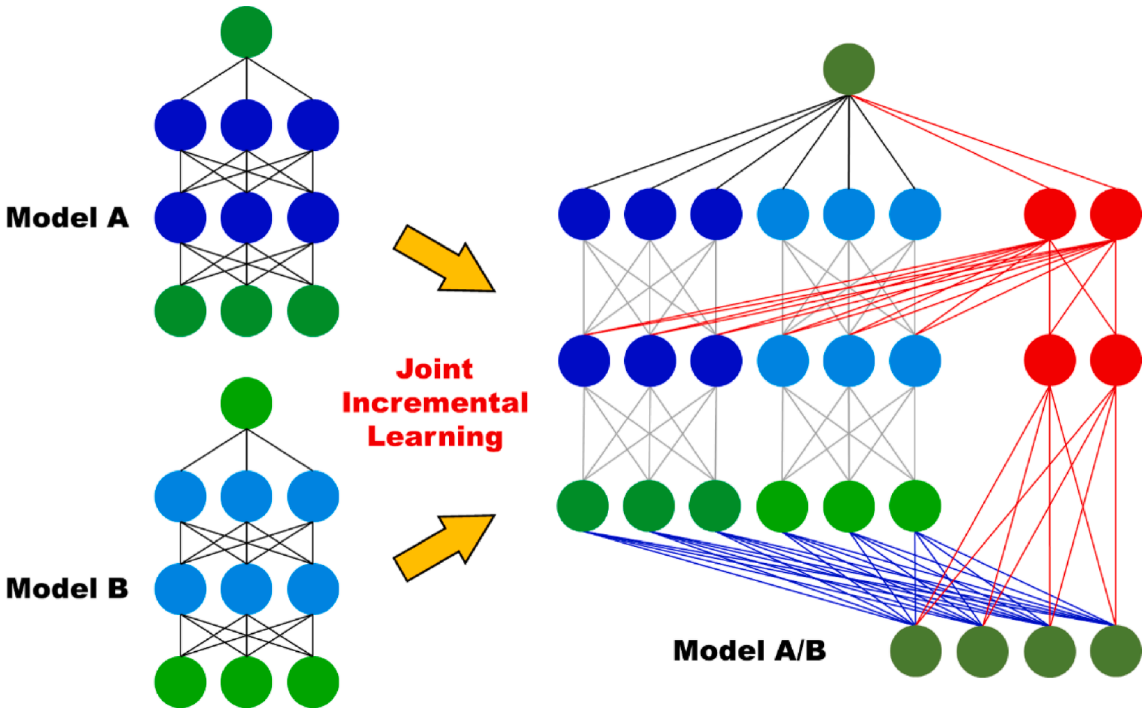

Fig. 4. Joint incremental learning network for CO_2 solubility in aqueous amine blends.

net training techniques [67], as depicted in Fig. 4, the linear layer (colored in blue) was then attached to the combined JILN model between the input layer **x** and the mono-solvent sub-model *j*. This practice is believed to be effective to solve the problem of distribution shifts.

4.3. Joint incremental learning network (JILN)

The JILN model combines the concepts of both joint learning (i.e., by combining multiple models laterally) and incremental learning (i.e., by increasing the number of hidden neurons as depicted in Fig. 2). It can be seen that the multiple well pre-trained FNN models with previously-learnt knowledge, i.e., weights and biases, are preserved and incorporated in the new FNN structure by layer-wisely sharing the hierarchical hidden information with the expanded neurons, which are colored in red in Fig. 4. Notice that this information distribution goal may be realized by layer-wisely and laterally connecting the existing hidden layer(s) with an additional expanded one [62,63]. To be more specific, the matrix–vector multiplication in each hidden layer of the expanded block can be expressed as:

$$\mathbf{h}_i^{(k)} = \phi\left(\mathbf{W}_i^{(k)}\mathbf{h}_{i-1}^{(k)} + \sum_j \mathbf{W}_i^{(j:k)}\mathbf{h}_i^{(j)} + \mathbf{b}_i^{(k)}\right) \tag{6}$$

where *i* is the index defined identically to that given in Eq. (3), while *k* represents the expanded network block (colored in red in Fig. 4) obtained during the joint incremental learning steps. To model the CO_2 solubility in amine mixtures using the JILN method, the index *j* was used to distinguish the mono-solvent models (colored in blues in Fig. 4) which were pre-trained with the corresponding datasets. Notice that $\mathbf{W}_i^{(j:k)}$ denotes the weight matrix of the lateral connections (expressed with symbol :) between layer *i* in block *j* and layer *i* in block *k*. The definition of the remaining matrix and vector are the same as those used for Eq. (3). Finally, ϕ is also the nonlinear activation operator. Based on the training procedure depicted in Fig. 3, the JILN model is then end-to-end trained on the basis of the dataset of amine mixtures in a supervised manner.

After joint incremental learning, the input–output relationships for bi-solvent models may be expressed as Eq. (7), where the concentrations of the individual amines in the aqueous solution, i.e., $C_{A,0}$ and $C_{B,0}$, are simultaneously considered in order to adequately represent the feature contributions and learn the interactions between the amines involved. Such functional relationship is analogous to that based on the semi-empirical methods [31,32,54].

$$\alpha_{CO_2} = f\left(T, C_{A,0}, C_{B,0}, P_{CO_2}\right) \tag{7}$$

5. Case studies

5.1. Experimental data of CO_2 solubility

5.1.1. Data acquisition

Five extensively studied amine solvents with abundant experimental data were adopted to construct the mono-solvent models, i.e., base models for joint incremental learning. The CO_2 solubility data in the amine solutions of MEA [5,8,56,68–72], DEA [73–75], MDEA [71,72,76–82], AMP [3,22,83–89] and PZ [90–95] were taken from published papers, and further details of these datasets, i.e., the ranges of temperature (°C), the amine concentration (wt%), the partial pressure (kPa), the equilibrium solubility (mol CO_2/mol amine) and the numbers of data, are also presented in Table 3. It can be observed that the ranges of the above parameters vary widely.

To demonstrate the effectiveness of the proposed modeling approach, the CO_2 solubility data of six bi-solvent aqueous amines, i.e., MEA/MDEA [68,72,96,97], DEA/MDEA [68,96,98–101], DEA/AMP [86,99,101–104], MDEA/AMP [31,87,105,106], MDEA/PZ [106–108] and AMP/PZ [84,88,109–111], were also gathered from the published works. The technical analyses of some of these bi-solvent blends, e.g., MEA/MDEA or MDEA/PZ, in pilot tests showed promising potentials, that is, the blended solutions may be more effective for energy-saving and absorption-enhancing purposes [29,30]. These collected VLE datasets are summarized in Table 4.

Table 3
Experimental data of CO_2 solubility in the single amine solutions.

Amine solutions	T (°C)	C_{amine} (wt%)	P_{CO_2} (kPa)	α_{CO_2} (mol/mol)	N_{data}
MEA	25–170	6.1–60	0.1–19936	0.211–2.152	711
DEA	0–205	5.3–84	0.689–6895	0.08–2.34	428
MDEA	25–200	5–75	1.7–7565	0.1–1.833	382
AMP	20–80	8.9–50	1.59–6987	0.126–1.126	359
PZ	15–120	1–50	0.115–9560	0.073–2.61	210

Table 4
Experimental data of CO_2 solubility in bi-solvent amine blends.

Amine mixtures	T (°C)	C_{amine} (wt%)	P_{CO_2} (kPa)	α_{CO_2} (mol/mol)	N_{data}
MEA/MDEA	25–180	10–24/6–25	0.724–19934	0.125–1.473	221
DEA/MDEA	30–180	5.3–35.7/6–35.7	1.1–3845	0.038–1.119	297
DEA/AMP	30–100	1.5–31.5/5–28.5	1.021–2908	0.262–1.2	227
MDEA/AMP	25–80	11.8–25/8.9–25	0.11–6400	0.439–1.856	106
MDEA/PZ	30–120	11.8–48/2–16.8	2.509–11880	0.2582–1.8714	277
AMP/PZ	30–120	17.8–48/2–12.9	0.442–1464	0.131–1.029	426

5.1.2. Data preprocessing

In machine learning applications, the first step is often rescaling the raw data so as to enhance training performance. In this study, the min–max normalization method (see Eq. (8) below) was adopted to map all input and output variables to interval [0,1] before the subsequent modeling steps.

$$z = \frac{x - min(x)}{max(x) - min(x)} \tag{8}$$

The next usual practice adopted to process each rescaled dataset was to partition it into the modeling and testing subsets. The former was further separated into two groups for training and validation respectively. The ratio of modeling to testing sample sizes was always set to be

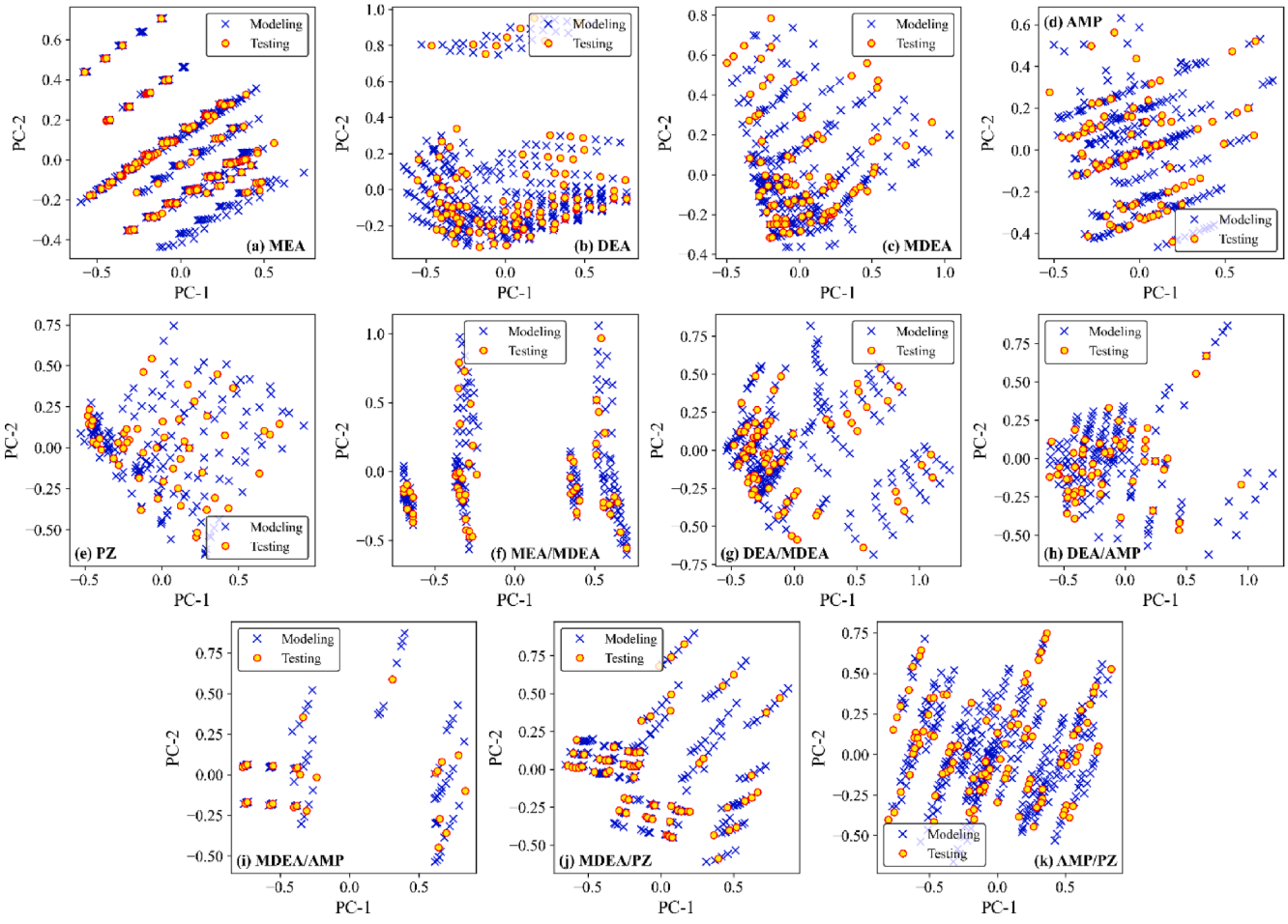

Fig. 5. Distributions of modeling and testing data in two-dimensional PCA spaces.

3 in this study, while a fixed ratio of training to validation sample numbers was also set to be 3 for all cases. The training, validation and testing data were randomly sampled, and their distributions were then analyzed by the standard principal component analysis (PCA). The corresponding four- or five-dimensional feature spaces were reduced to two-dimensional ones for better visualizations. From Fig. 5, one can see that the distributions of data used respectively for modeling and testing are quite similar in the two-dimensional PCA spaces, which implied that the above-mentioned data partition strategies are suitable for model building and validation at least in the present studies.

5.2. Network designs and training

Both ANN and JILN models were built by open-source Keras software in Python environment, and a personal computer with Intel Core i7-7700 CPU 3.60 GHz was used to train all models. Since the number of parameters in these models was relatively small, every training session was completed in only a few minutes. The fully-connected FNNs with 1 or 2 hidden layer(s) was adopted in all cases under consideration [112], and the nonlinear transformation performed by the hidden-state vectors was facilitated with the hyperbolic tangent function. Consequently, the Glorot-normal initializer was chosen for generating properly initialized weights and biases that are normally distributed around zero [113]. In this study, the number of trainable parameters was limited within the range of between 1 and 300. 5 to 40 nodes and 1 to 13 node(s) were thus chosen for building the 1- and 2-layer ANNs respectively, while at most 8 nodes were adopted for fabricating the JILNs. The loss function adopted for backpropagations was the mean absolute error, and the Adam optimizer was utilized to minimize this loss via updating network parameters. To avoid overfitting during model training, the above loss function was modified by incorporating the ridge regularization penalty with a factor of 0.0001.

To ensure convergence of the training process, the largest iteration number of the gradient descent was always set to be a very large number (50000) and a small learning rate of 0.001 in each optimization run, and an early-stopping mechanism was also put in place with a patience setting of 3000 iterations. From the computation results, one can observe that almost all training sessions stopped early at around 15000–40000 iterations, which indicates the models gained no further improvement in the last 3000 updates.

5.3. Evaluation of model performances

To evaluate the effectiveness of the proposed method, the effect(s) of increasing the number of hidden neurons on the prediction capability of every trained and validated ANN model was thoroughly investigated. Notice that this extra neuron addition is in fact equivalent to introducing more neurons during the incremental learning stage. Four metrics, i.e., R-squared (R^2), root mean squared error (RMSE), mean absolute error (MAE) and mean absolute percentage error (MAPE), were adopted to evaluate the differences between the predicted values ($\hat{y}$) and the real data (y). For the sake of completeness, the mathematical formula of these well-known metrics are duplicated below in Eqs. (9)–(12).

$$R^2 = 1 - \frac{\sum_n (\hat{y}_n - y_n)^2}{\sum_n (\bar{y} - y_n)^2} \tag{9}$$

$$\mathrm{RMSE} = \sqrt{\frac{1}{N}\sum_{n=1}^{N} (\hat{y}_n - y_n)^2} \tag{10}$$

$$\mathrm{MAE} = \frac{1}{N}\sum_{n=1}^{N} |\hat{y}_n - y_n| \tag{11}$$

$$\mathrm{MAPE} = \frac{100\%}{N}\sum_{n=1}^{N} \left|\frac{\hat{y}_n - y_n}{y_n}\right| \tag{12}$$

5.4. Results and discussions

5.4.1. Performances of mono-solvent models

To implement the proposed JILN method, the first step is to make sure that the base models are able to capture the correct mechanistic knowledge in order to accurately predict the CO_2 solubility in mono-solvent aqueous mixtures. Two hyper-parameters, i.e., the number of hidden layers and the number of hidden nodes (at each layer), were adjusted to search for the optimal base models. As mentioned earlier, the number of hidden layers was 1 or 2, and 1 to 8 hidden nodes can be included in each layer. The testing MAPEs of five mono-solvent models with different structures were given in Table 5. It can be seen that the 2-layer models generally outperformed their 1-layer counterparts, especially when the number of hidden nodes was greater than 3. From these testing results, it should be concluded that the optimal mono-solvent models most probably were 2-layer ANNs with 6–9 hidden nodes. Notice especially that the MAPEs of these optimal mono-solvent models were within the range of 3.6–7.7 %, which should be considered to be

Table 5
Testing MAPEs of mono-solvent models with different network structures.

No. of nodes	Mean absolute percentage error (MAPE) on testing sets									
	MEA models		DEA models		MDEA models		AMP models		PZ models	
	1-layer	2-layer	1-layer	2-layer	1-layer	2-layer	1-layer	2-layer	1-layer	2-layer
1	14.611	14.911	33.543	33.556	44.464	39.874	31.203	22.035	21.349	20.550
2	10.560	10.976	32.021	28.251	18.233	21.688	17.179	11.314	12.517	10.036
3	9.956	7.619	18.120	23.062	16.938	10.306	30.885	16.162	9.996	4.454
4	10.107	4.735	17.813	10.878	17.396	10.898	7.314	4.526	7.340	5.125
5	7.111	4.519	13.729	14.510	16.277	9.326	17.584	6.184	7.275	4.205
6	6.668	4.226	13.482	9.385	16.237	**7.318**	7.138	5.130	5.196	4.552
7	6.413	**3.573**	14.386	8.453	17.061	9.889	19.114	**3.712**	7.738	**3.799**
8	6.060	3.974	16.202	8.857	15.746	8.626	16.781	5.318	6.000	4.066
9	6.638	4.011	13.251	**7.703**	13.918	8.878	8.164	5.220	5.241	4.502
10	6.626	4.073	26.572	8.323	13.480	8.088	6.136	4.456	6.324	4.714

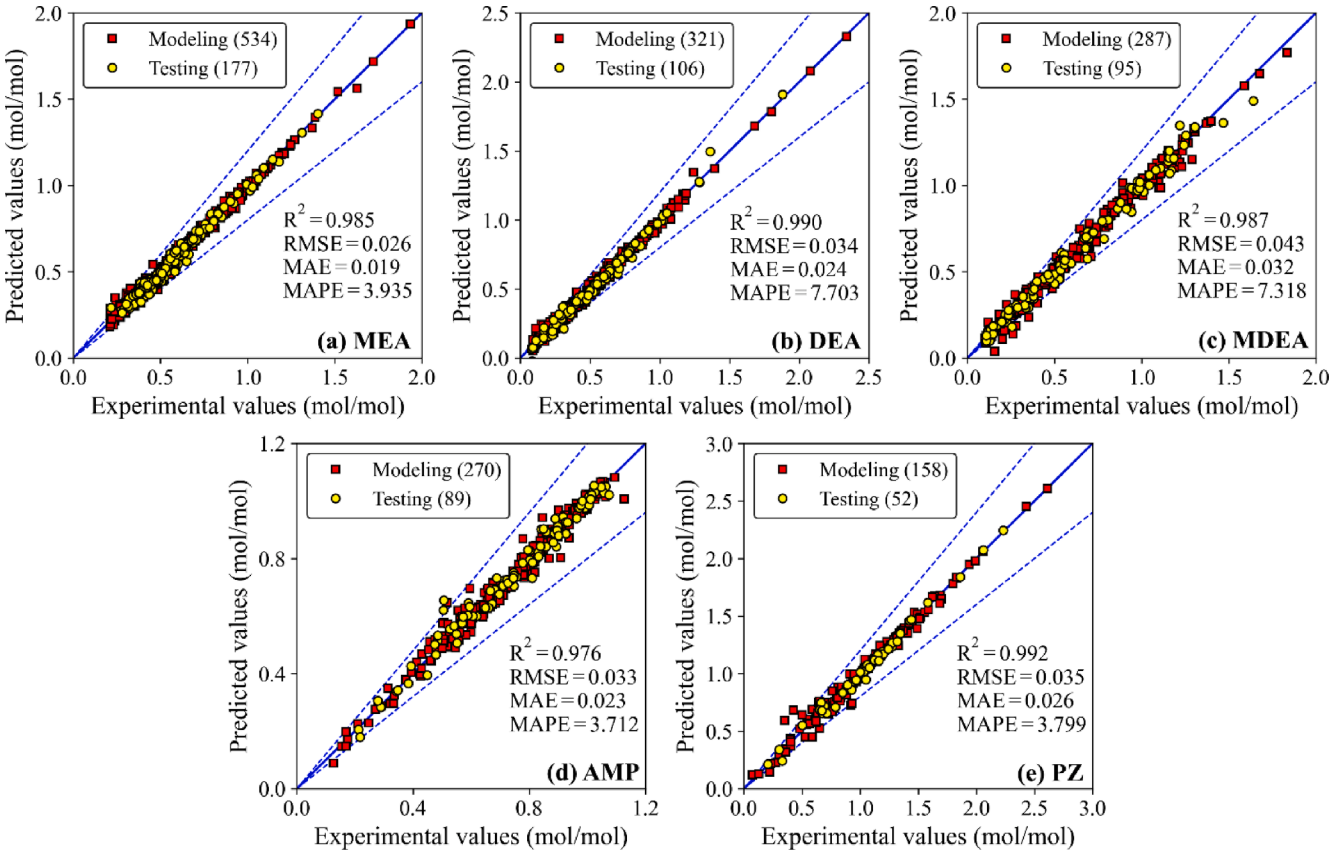

Fig. 6. The prediction performances of the mono-solvent models.

extremely accurate if compared with the semi-empirical models [8,83,90,98] or the conventional ML models [21].

The modeling and testing parity plots of above-mentioned optimal models are also given in Fig. 6. It can be clearly observed that the prediction errors in both cases were very small (signified with red squares and yellow points respectively), and that nearly all prediction errors were within 20 % (shown by the blue dash lines). The values of R^2, RMSE, MAE and MAPE are also provided all the subplots of Fig. 6. Notice that (1) the red squares and yellow points both scattered near the diagonals, (2) most of the R^2 scores were greater than 0.985, and (3) the RMSEs and MAEs were within the ranges of 0.023–0.046 mol/mol and 0.017–0.034 mol/mol respectively. It should be also noted that the cross validations of RMSEs and MAEs are useful for identifying the outlier effects. Since the ranges of RMSEs and MAEs were very close to one another, the outlier effects on these metrics should be negligible. One can therefore conclude that the mechanistic knowledge of CO_2 solubility in these mono-solvent systems can be correctly captured by the aforementioned models.

5.4.2. *Performances of bi-solvent models*

In this study, the JILN models were compared with the 1-layer and 2-layer ANN counterparts. Notice that a large fraction of the model parameters used in JILNs, i.e., the ones embedded in the base models, were kept frozen during the joint incremental learning stage. Since the modeling approaches are not the same, it would be unfair to compare models on the basis of hidden neuron sizes. Consequently, they were compared on the basis of the unified standard of number of trainable parameters.

The testing MAPEs for the six bi-solvent cases were given in Fig. 7. One can observe from Fig. 7 that the prediction errors of JILN models (shown in green diamonds) were much smaller than those of their ANN counterparts (shown in red triangles and blue points) when almost the same trainable parameter sizes were used for modeling in these three different cases. Notice that similar trends found in the mono-solvent cases can also be observed here, i.e., the 2-layer ANNs in general outperformed their 1-layer counterparts. Although the trainable parameter sizes of JILN models were slightly greater than those of the conventional ANN counterparts if identical node numbers were adopted, these weights and biases in JILN can be more easily trained since most of them were guided by the hierarchical features of the base models with insightful mechanistic knowledge. From the testing results plotted in Fig. 7, it can be observed that the MAPEs of JILN models were close to or even smaller than 5 %, while those of 1- and 2-layer ANNs were much greater than the value of 5 %. It can be seen that the prediction performances of conventional ANN models were restricted by the datasets of bi-solvent mixtures, where the testing MAPEs won't significantly decrease even the trainable parameter sizes increase. On the other hand, partially driven by the inherent knowledge of the mono-solvent datasets, the JILN models were able to overcome such obstacles and produced more accurate predictions. It can thus be concluded that the knowledge

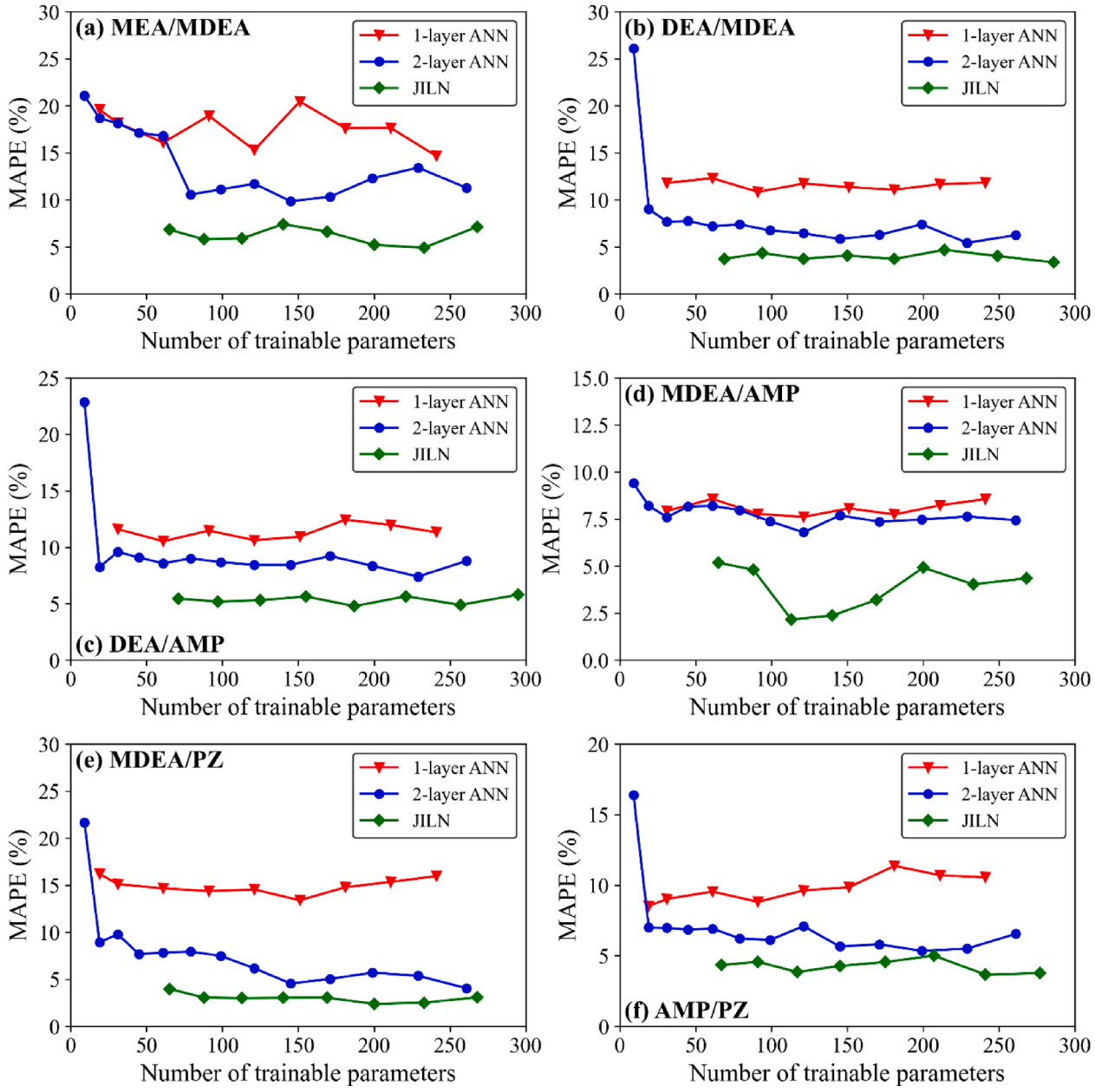

Fig. 7. The testing results of bi-solvent models with different number of trainable parameters.

Table 6
Testing results of ANN- and JILN-based bi-solvent models.

Aqueous mixtures	Optimal models	Model testing results			
		R^2	RMSE	MAE	MAPE
MEA/MDEA	9-node ANN	0.956	0.072	0.045	9.852
	7-node JILN	0.985	0.042	0.023	4.913
DEA/MDEA	12-node ANN	0.981	0.036	0.024	5.428
	8-node JILN	0.992	0.026	0.015	3.354
DEA/AMP	12-node ANN	0.911	0.054	0.039	7.396
	5-node JILN	0.945	0.041	0.027	4.779
MDEA/AMP	8-node ANN	0.944	0.070	0.050	6.791
	3-node JILN	0.992	0.034	0.021	2.162
MDEA/PZ	13-node ANN	0.987	0.037	0.025	4.047
	6-node JILN	0.995	0.024	0.017	2.382
AMP/PZ	11-node ANN	0.971	0.036	0.026	5.348
	7-node JILN	0.983	0.028	0.019	3.665

The number of nodes for JILN models refers to the expanded nodes rather than those of the base models.

embedded in the mono-solvent base models are indeed useful and can produce positive effects on the knowledge transfer and incremental learning of bi-solvent models.

The testing results of the optimal 2-layer ANN and JILN models were listed in Table 6 to facilitate further discussions. It can be seen that all testing MAPEs of JILN models lie within the interval [2.162 %, 4.913 %], which is a much narrower range if compared with that of 2-layer ANN models, i.e., [4.047 %, 9.852 %]. This comparison implies a 31–68 % reduction in prediction errors. Also, the MAPEs of JILN models were much smaller than those of the conventional empirical models reported in literatures [31,98,106]. Finally, notice that the testing RMSEs and MAEs of JILN models were within the ranges of 0.024–0.042 mol/mol and 0.015–0.023 mol/mol respectively, which are much smaller than the corresponding values of 2-layer ANN model, i.e., 0.034–0.072 mol/mol and 0.024–0.050 mol/mol. Based on the above analyses, it may be concluded that the JILN modeling approach is more effective and better suited to enhance the model performances if similar dataset sizes are available for thermodynamic property modeling.

The parity plots of optimal JILN-based bi-solvent models are presented in Fig. 8. Since the modeling and testing data points were closely located along the diagonals, one can confidently deduce that the prediction accuracies were at extremely high levels. More specifically, notice that the absolute prediction errors were almost all within 20 %. For further error analysis, the prediction results generated with the mono-solvent models are also given in Fig. 8 in the forms of pink plus and green cross symbols. Since the mono-solvent models are not able to take the concentration effects of the other amine in the mixture into consideration, some predicted values of the mono-solvent models are bound to significantly deviate from the experimental values of bi-solvent mixtures. Nevertheless, it should be pointed out that the predictions of mono-solvent models were already quite accurate because, theoretically speaking, the bi-solvent systems may be regarded as combinations of the corresponding mono-solvent ones with additional interactions. This observation indicates that the knowledge stored in the base models can be used as the foundation for meaningful extrapolation, and the expanded network blocks are certainly well guided by these laterally shared hierarchical features.

6. Conclusions

Accurate vapor–liquid equilibrium (VLE) models are crucial for reliable process simulation analyses and designs. In order to improve the CO_2 capture processes, there is a real need to search for better amine solvents and/or blends to enhance absorption efficiency and reduce energy consumption. To address this issue, the CO_2 solubility in aqueous amine solutions and mixtures have been accurately predicted with the proposed JILN model. Furthermore, this model can be very useful for further estimations of other important thermodynamic and transport properties. Although the machine learning (ML) techniques have been widely studied and used for VLE modeling, the traditional case-by-case training strategies are usually laborious and computationally intensive. Based on the concepts of joint and incremental learning, an alternative structure was proposed for the modeling of CO_2 solubility in six different aqueous bi-amine mixtures. With this novel modeling approach, the useful knowledge embedded in the mono-solvent base models were proven by numerical experiments to be useful for the property learning tasks of multi-solvent mixtures.

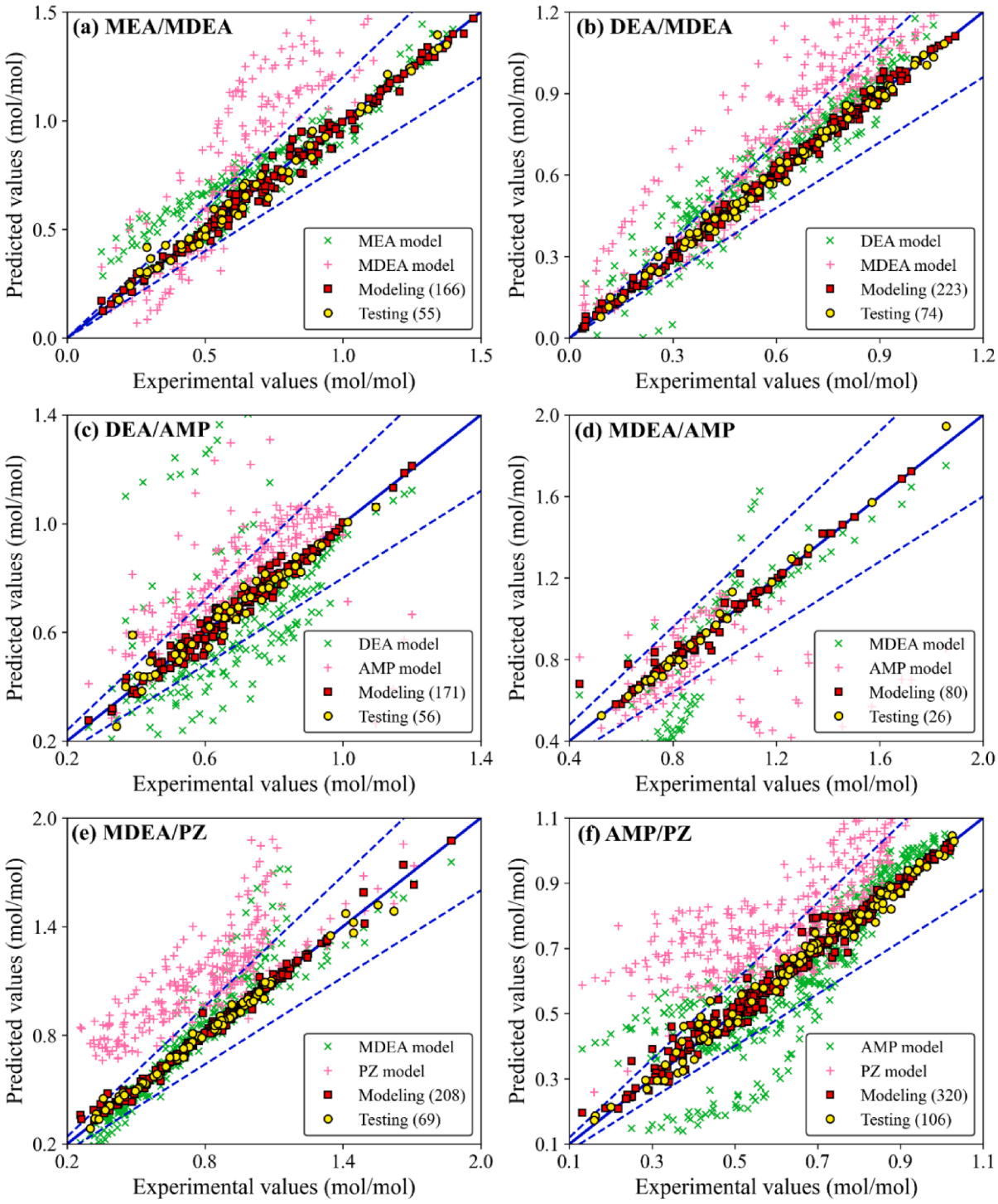

Fig. 8. The performances of mono-solvent base models and bi-solvent JILN models tested by the datasets of amine mixtures.

CRediT authorship contribution statement

Yu-Da Hsiao: Conceptualization, Methodology, Investigation, Software, Data curation, Visualization, Writing – original draft. **Chuei-Tin Chang:** Investigation, Resources, Supervision, Writing – review & editing.

Declaration of Competing Interest

The authors declare that they have no known competing financial interests or personal relationships that could have appeared to influence the work reported in this paper.

Data availability

Data will be made available on request.

References

[1] H. Ahn, M. Luberti, Z. Liu, S. Brandani, Process configuration studies of the amine capture process for coal-fired power plants, J. Greenh. Gas Control 16 (2013) 29–40.

[2] T.N. Borhani, M. Wang, Role of solvents in CO_2 capture processes: the review of selection and design methods, Renew. Sustain. Energy Rev. 114 (2019), 109299.

[3] M. Sharif, T. Zhang, X. Wu, Y. Yu, Z. Zhang, Evaluation of CO_2 absorption performance by molecular dynamic simulation for mixed secondary and tertiary amines, J. Greenh. Gas Control 97 (2020), 103059.

[4] H. Liu, C. Chan, P. Tontiwachwuthikul, R. Idem, Analysis of CO_2 equilibrium solubility of seven tertiary amine solvents using thermodynamic and ANN models, Fuel 249 (2019) 61–72.

[5] H.S. Park, K.B. Lee, J.C. Hyun, S.H. Kim, Correlation and prediction of the solubility of carbon dioxide in aqueous alkanolamine and mixed alkanolamine solutions, Ind. Eng. Chem. Res. 41 (2002) 1658–1665.

[6] R.D. Deshmukh, A.E. Mather, A mathematical model for equilibrium solubility of hydrogen sulfide and carbon dioxide in aqueous alkanolamine solutions, Chem. Eng. Sci. 36 (1981) 355–362.

[7] Y. Zhang, H. Que, C.-C. Chen, Thermodynamic modeling for CO_2 absorption in aqueous MEA solution with electrolyte NRTL model, Fluid Ph. Equilibria 311 (2011) 67–75.

[8] U.E. Aronu, S. Gondal, E.T. Hessen, T. Haug-Warberg, A. Hartono, K.A. Hoff, H. F. Svendsen, Solubility of CO_2 in 15, 30, 45 and 60 mass% MEA from 40 to 120°C and model representation using the extended UNIQUAC framework, Chem. Eng. Sci. 66 (2011) 6393–6406.

[9] G. Chen, X. Luo, H. Zhang, K. Fu, Z. Liang, W. Rongwong, P. Tontiwachwuthikul, R. Idem, Artificial neural network models for the prediction of CO_2 solubility in aqueous amine solutions, J. Greenh. Gas Control 39 (2015) 174–184.

[10] L. Helei, P. Tantikhajorngosol, C. Chan, P. Tontiwachwuthikul, Technology development and applications of artificial intelligence for post-combustion carbon dioxide capture: critical literature review and perspectives, J. Greenh. Gas Control 108 (2021), 103307.

[11] K. Zhang, J. Wu, H. Yoo, Y. Lee, Machine learning-based approach for tailor-made design of ionic liquids: application to CO_2 capture, Sep. Purif. Technol. 275 (2021), 119117.

[12] M. Hosseinpour, M.J. Shojaei, M. Salimi, M. Amidpour, Machine learning in absorption-based post-combustion carbon capture systems: a state-of-the-art review, Fuel 353 (2023), 129265.

[13] F. Li, J. Zhang, E. Oko, M. Wang, Modelling of a post-combustion CO_2 capture process using neural networks, Fuel 151 (2015) 156–163.

[14] A. Nuchitprasittichai, S. Cremaschi, Optimization of CO_2 capture process with aqueous amines using response surface methodology, Comput. Chem. Eng. 35 (2011) 1521–1531.

[15] N. Sipöcz, F.A. Tobiesen, M. Assadi, The use of artificial neural network models for CO_2 capture plants, Appl. Energy 88 (2011) 2368–2376.

[16] Y. Wu, Q. Zhou, C.W. Chan, A comparison of two data analysis techniques and their applications for modeling the carbon dioxide capture process, Eng. Appl. Artif. Intel. 23 (2010) 1265–1276.

[17] K. Golzar, H. Modarress, S. Amjad-Iranagh, Evaluation of density, viscosity, surface tension and CO2 solubility for single, binary and ternary aqueous solutions of MDEA, PZ and 12 common ILs by using artificial neural network (ANN) technique, J. Greenh. Gas Control 53 (2016) 187–197.

[18] S.A. Mazari, A.R. Siyal, N.H. Solangi, S. Ahmed, G. Griffin, R. Abro, N. M. Mubarak, M. Ahmed, N. Sabzoi, Prediction of thermo-physical properties of 1-butyl-3-methylimidazolium hexafluorophosphate for CO_2 capture using machine learning models, J. Mol. Liq. 327 (2021), 114785.

[19] B.K. Mondal, S.S. Bandyopadhyay, A.N. Samanta, Equilibrium solubility and enthalpy of CO2 absorption in aqueous bis(3-aminopropyl) amine and its mixture with MEA, MDEA, AMP and K2CO3, Chem. Eng. Sci. 170 (2017) 58–67.

[20] A. Tatar, A. Barati-Harooni, A. Najafi-Marghmaleki, A. Mohebbi, M.M. Ghiasi, A. H. Mohammadi, A. Hajinezhad, Comparison of two soft computing approaches for predicting CO_2 solubility in aqueous solution of piperazine, J. Greenh. Gas Control 53 (2016) 85–97.

[21] H. Yarveicy, M.M. Ghiasi, A.H. Mohammadi, Performance evaluation of the machine learning approaches in modeling of CO_2 equilibrium absorption in piperazine aqueous solution, J. Mol. Liq. 255 (2018) 375–383.

[22] H. Pahlavanzadeh, S. Nourani, M. Saber, Experimental analysis and modeling of CO2 solubility in AMP (2-amino-2-methyl-1-propanol) at low CO2 partial pressure using the models of Deshmukh-Mather and the artificial neural network, J. Chem. Thermodyn. 43 (2011) 1775–1783.

[23] N. Daneshvar, M.T.Z. Moattar, M.A. Abdi, S. Aber, Carbon dioxide equilibrium absorption in the multi-component systems of CO_2 + TIPA + MEA + H_2O, CO_2 + TIPA + Pz + H_2O and CO_2 + TIPA + H_2O at low CO_2 partial pressures: experimental solubility data, corrosion study and modeling with artificial neural network, Sep. Purif. Technol. 37 (2004) 135–147.

[24] H. Liu, V.K.H. Chan, P. Tantikhajorngosol, T. Li, S. Dong, C. Chan, P. Tontiwachwuthikul, Novel machine learning model correlating CO_2 equilibrium solubility in three tertiary amines, Ind. Eng. Chem. Res. 61 (2022) 14020–14032.

[25] H. Saghafi, M. Arabloo, Modeling of CO_2 solubility in MEA, DEA, TEA, and MDEA aqueous solutions using AdaBoost-decision tree and artificial neural network, J. Greenh. Gas Control 58 (2017) 256–265.

[26] Z. Zhang, H. Li, H. Chang, Z. Pan, X. Luo, Machine learning predictive framework for CO_2 thermodynamic properties in solution, J. CO2 Util. 26 (2018) 152–159.

[27] B. Aghel, S. Janati, S. Wongwises, M.S. Shadloo, Review on CO_2 capture by blended amine solutions, J. Greenh. Gas Control 119 (2022), 103715.

[28] Y. Artanto, J. Jansen, P. Pearson, T. Do, A. Cottrell, E. Meuleman, P. Feron, Performance of MEA and amine-blends in the CSIRO PCC pilot plant at Loy Yang Power in Australia, Fuel 101 (2012) 264–275.

[29] R. Idem, M. Wilson, P. Tontiwachiwuthikul, A. Chakma, A. Veawab, A. Aroonwilas, D. Gelowitz, Pilot plant studies of the CO_2 capture performance of aqueous MEA and mixed MEA/MDEA solvents at the University of Regina CO_2 capture technology development plant and the boundary dam CO_2 capture demonstration plant, Ind. Eng. Chem. Res. 45 (2006) 2414–2420.

[30] C. Nwaoha, P. Tontiwachwuthikul, A. Benamor, CO_2 capture from water-gas shift process plant: comparative bench-scale pilot plant investigation of MDEA-PZ blend vs novel MDEA activated by 1,5-diamino-2-methylpentane, J. Greenh. Gas Control 82 (2019) 218–228.

[31] G. Kontos, K. Leontiadis, I. Tsivintzelis, CO_2 solubility in aqueous solutions of blended amines: experimental data for mixtures with MDEA, AMP and MPA and modeling with the modified Kent-Eisenberg model, Fluid Ph. Equilibria 570 (2023), 113800.

[32] H. Suleman, A.S. Maulud, P.L. Fosbøl, Q. Nasir, R. Nasir, M.Z. Shahid, M. Nawaz, M. Abunowara, A review of semi-empirical equilibrium models for CO_2-alkanolamine-H_2O solutions and their mixtures at high pressure, J. Environ. Chem. Eng. 9 (2021), 104713.

[33] S.J. Hwang, H. Kim, K.S. Lee, Prediction of VLE for aqueous blended amines using VLE models of single amines, J. Greenh. Gas Control 49 (2016) 250–258.

[34] W. Zheng, Q. Luo, S. Liu, N. Wang, X. Luo, H. Gao, Z. Liang, New method of kinetic modeling for CO_2 absorption into blended amine systems: a case of MEA/EAE/3DEA1P trisolvent blends, AIChE J 68 (2022) e17628.

[35] D. Bastani, M.E. Hamzehie, F. Davardoost, S. Mazinani, A. Poorbashiri, Prediction of CO_2 loading capacity of chemical absorbents using a multi-layer perceptron neural network, Fluid Ph. Equilibria 354 (2013) 6–11.

[36] M.E. Hamzehie, S. Mazinani, F. Davardoost, A. Mokhtare, H. Najibi, B. Van der Bruggen, S. Darvishmanesh, Developing a feed forward multilayer neural network model for prediction of CO_2 solubility in blended aqueous amine solutions, J. Nat. Gas Eng. 21 (2014) 19–25.

[37] M.M. Ghiasi, A. Hajinezhad, H. Yousefi, A.H. Mohammadi, CO_2 loading capacity of DEA aqueous solutions: modeling and assessment of experimental data, J. Greenh. Gas Control 56 (2017) 289–301.

[38] S.C. Balchandani, A. Dey, Prediction of CO_2 solubility in potential blends of ionic liquids with alkanolamines using statistical non-rigorous and ANN based modeling: a comprehensive simulation study for post combustion CO_2 capture, Int. Commun. Heat Mass Transf. 132 (2022), 105866.

[39] M. Afkhamipour, M. Mofarahi, T.N.G. Borhani, M. Zanganeh, Prediction of heat capacity of amine solutions using artificial neural network and thermodynamic models for CO_2 capture processes, Heat Mass Transf. 54 (2017) 855–866.

[40] P. Haratipour, A. Baghban, A.H. Mohammadi, S.H.H. Nazhad, A. Bahadori, On the estimation of viscosities and densities of CO2-loaded MDEA, MDEA + AMP, MDEA + DIPA, MDEA + MEA, and MDEA + DEA aqueous solutions, J. Mol. Liq. 242 (2017) 146–159.

[41] A. Aminian, B. ZareNezhad, Predicting the shear viscosity of carbonated aqueous amine solutions and their blends by using an artificial neural network model, Energ. Fuel 34 (2020) 16389–16400.

[42] N.S. Mousavi, B. Vaferi, A. Romero-Martínez, Prediction of surface tension of various aqueous amine solutions using the UNIFAC model and artificial neural networks, Ind. Eng. Chem. Res. 60 (2021) 10354–10364.

[43] S. Dong, H. Quan, D. Zhao, H. Li, J. Geng, H. Liu, Generic AI models for mass transfer coefficient prediction in amine-based CO_2 absorber, Part I: BPNN model, Chem. Eng. Sci. 264 (2022), 118165.

[44] H. Quan, S. Dong, D. Zhao, H. Li, J. Geng, H. Liu, Generic AI models for mass transfer coefficient prediction in amine-based CO2 absorber. Part II: RBFNN and RF model, AIChE J. 69 (2022) e17904.
[45] D. Goldstein, M. Heyer, D. Jakobs, E.S. Schultz, L.T. Biegler, Multilevel surrogate modeling of an amine scrubbing process for CO_2 capture, AIChE J 68 (2022) e17705.
[46] X. Yang, R.J. Rees, W. Conway, G. Puxty, Q. Yang, D.A. Winkler, Computational modeling and dimulation of CO_2 capture by aqueous amines, Chem. Rev. 117 (2017) 9524–9593.
[47] S. Laribi, L. Dubois, G. De Weireld, D. Thomas, Study of the post-combustion CO_2 capture process by absorption-regeneration using amine solvents applied to cement plant flue gases with high CO_2 contents, J. Greenh. Gas Control 90 (2019), 102799.
[48] P.V. Danckwerts, The reaction of CO_2 with ethanolamines, Chem. Eng. Sci. 34 (1979) 443–446.
[49] M. Caplow, Kinetics of carbamate formation and breakdown, J. Am. Chem. Soc. 90 (1968) 6795–6803.
[50] P.M.M. Blauwhoff, G.F. Versteeg, W.P.M. Van Swaaij, A study on the reaction between CO_2 and alkanolamines in aqueous solutions, Chem. Eng. Sci. 38 (1984) 1411–1429.
[51] T.L. Donaldson, Y.N. Nguyen, Carbon dioxide reaction kinetics and transport in aqueous amine membranes, Ind. Eng. Chem. Fund. 19 (1980) 260–266.
[52] A. Aboudheir, P. Tontiwachwuthikul, A. Chakma, R. Idem, Kinetics of the reactive absorption of carbon dioxide in high CO_2-loaded, concentrated aqueous monoethanolamine solutions, Chem. Eng. Sci. 58 (2003) 5195–5210.
[53] M.K. Aroua, R. Mohd Salleh, Solubility of CO_2 in aqueous piperazine and its modeling using the Kent-Eisenberg approach, Chem. Eng. Technol. 27 (2004) 65–70.
[54] M.N. Hassankiadeh, A. Jahangiri, Application of aqueous blends of AMP and piperazine to the low CO_2 partial pressure capturing: new experimental and theoretical analysis, Energy 165 (2018) 164–178.
[55] A. Chakma, A. Meisen, Improved Kent-Eisenberg model for predicting CO2 solubilities in aqueous diethanolamine (DEA) solutions, Gas Sep. Purif. 4 (1990) 37–40.
[56] J.H. Jones, H.R. Froning, E.E. Claytor Jr, Solubility of acidic gases in aqueous monoethanolamine, J. Chem. Eng. Data 4 (1959) 85–92.
[57] A. Penttilä, C. Dell'Era, P. Uusi-Kyyny, V. Alopaeus, The Henry's law constant of N2O and CO2 in aqueous binary and ternary amine solutions (MEA, DEA, DIPA, MDEA, and AMP), Fluid Ph. Equilibria 311 (2011) 59–66.
[58] A.V. Terekhov, G. Montone, J.K. O'Regan, Knowledge transfer in deep block-modular neural networks, in: Conference on Biomimetic and Biohybrid Systems, Springer, 2015, pp. 268–279.
[59] K. Chen, Deep and modular neural networks, Springer Handbook of Computational Intelligence, in, 2015, pp. 473–494.
[60] A.K. Malik, R. Gao, M.A. Ganaie, M. Tanveer, P.N. Suganthan, Random vector functional link network: recent developments, applications, and future directions, Appl. Soft Comput. 143 (2023), 110377.
[61] A.A. Rusu, N.C. Rabinowitz, G. Desjardins, H. Soyer, J. Kirkpatrick, K. Kavukcuoglu, R. Pascanu, R. Hadsell, Progressive neural networks, arXiv preprint, 2016.
[62] H.M. Fayek, L. Cavedon, H.R. Wu, Progressive learning: a deep learning framework for continual learning, Neural Netw. 128 (2020) 345–357.
[63] G.I. Parisi, R. Kemker, J.L. Part, C. Kanan, S. Wermter, Continual lifelong learning with neural networks: a review, Neural Netw. 113 (2019) 54–71.
[64] Y.-D. Hsiao, C.-T. Chang, Progressive learning for surrogate modeling of amine scrubbing CO_2 capture processes, Chem. Eng. Res. Des. 194 (2023) 653–665.
[65] X. Zhang, Y. Zou, S. Li, Enhancing incremental deep learning for FCCU end-point quality prediction, Inf. Sci. 530 (2020) 95–107.
[66] T. Han, C. Liu, R. Wu, D. Jiang, Deep transfer learning with limited data for machinery fault diagnosis, Appl. Soft Comput. 103 (2021), 107150.
[67] T. Chen, I. Goodfellow, J. Shlens, Net2Net: Accelerating learning via knowledge transfer, arXiv preprint, 2015.
[68] D.M. Austgen, G.T. Rochelle, C.-C. Chen, Model of vapor-liquid equilibria for aqueous acid gas-alkanolamine systems. 2. Representation of hydrogen sulfide and carbon dioxide solubility in aqueous MDEA and carbon dioxide solubility in aqueous mixtures of MDEA with MEA or DEA, Ind. Eng. Chem. Res. 30 (1991) 543–555.
[69] F.-Y. Jou, A.E. Mather, F.D. Otto, The solubility of CO_2 in a 30 mass percent monoethanolamine solution, Can. J. Chem. Eng. 73 (1995) 140–147.
[70] J.I. Lee, F.D. Otto, A.E. Mather, Solubility of carbon dioxide in aqueous diethanolamine solutions at high pressures, J. Chem. Eng. Data 17 (1972) 465–468.
[71] S. Ma'mun, R. Nilsen, H.F. Svendsen, Solubility of carbon dioxide in 30 mass% monoethanolamine and 50 mass% methyldiethanolamine solutions, J. Chem. Eng. Data 50 (2005) 630–634.
[72] K.-P. Shen, M.-H. Li, Solubility of carbon dioxide in aqueous mixtures of monoethanolamine with methyldiethanolamine, J. Chem. Eng. Data 37 (1992) 96–100.
[73] M.Z. Haji-Sulaiman, M.K. Aroua, A. Benamor, Analysis of equilibrium data of CO2 in aqueous solutions of diethanolamine (DEA), methyldiethanolamine (MDEA) and their mixtures using the modified Kent Eisenberg model, Chem. Eng. Res. Des. 76 (1998) 961–968.
[74] M.L. Kennard, A. Meisen, Solubility of carbon dioxide in aqueous diethanolamine solutions at elevated temperatures and pressures, J. Chem. Eng. Data 29 (1984) 309–312.
[75] J.D. Lawson, A.W. Garst, Gas sweetening data: equilibrium solubility of hydrogen sulfide and carbon dioxide in aqueous monoethanolamine and aqueous diethanolamine solutions, J. Chem. Eng. Data 21 (1976) 20–30.
[76] A. Chakma, A. Meisen, Solubility of carbon dioxide in aqueous methyldiethanolamine and N, N-bis (hydroxyethyl) piperazine solutions, Ind. Eng. Chem. Res. 26 (1987) 2461–2466.
[77] V. Ermatchkov, Á.-P.-S. Kamps, G. Maurer, Solubility of carbon dioxide in aqueous solutions of N-methyldiethanolamine in the low gas loading region, Ind. Eng. Chem. Res. 45 (2006) 6081–6091.
[78] F.-Y. Jou, A.E. Mather, F.D. Otto, Solubility of H_2S and CO_2 in aqueous methyldiethanolamine solutions, Ind. Eng. Chem. Process Des. Dev. 21 (1982) 539–544.
[79] Á.-P.-S. Kamps, A. Balaban, M. Jödecke, G. Kuranov, N.A. Smirnova, G. Maurer, Solubility of single gases carbon dioxide and hydrogen sulfide in aqueous solutions of N-methyldiethanolamine at temperatures from 313 to 393 K and pressures up to 7.6 MPa: new experimental data and model extension, Ind. Eng. Chem. Res. 40 (2001) 696–706.
[80] G. Kuranov, B. Rumpf, N.A. Smirnova, G. Maurer, Solubility of single gases carbon dioxide and hydrogen sulfide in aqueous solutions of N-methyldiethanolamine in the temperature range 313–413 K at pressures up to 5 MPa, Ind. Eng. Chem. Res. 35 (1996) 1959–1966.
[81] M.K. Park, O.C. Sandall, Solubility of carbon dioxide and nitrous oxide in 50 mass % methyldiethanolamine, J. Chem. Eng. Data 46 (2001) 166–168.
[82] S.-W. Rho, K.-P. Yoo, Solubility of CO_2 in aqueous methyldiethanolamine solutions, J. Chem. Eng. Data 42 (1997) 1161–1164.
[83] S.K. Dash, A.N. Samanta, S.S. Bandyopadhyay, (Vapour+liquid) equilibria (VLE) of CO2 in aqueous solutions of 2-amino-2-methyl-1-propanol: new data and modelling using eNRTL-equation, J. Chem. Thermodyn. 43 (2011) 1278–1285.
[84] S.K. Dash, A.N. Samanta, S.S. Bandyopadhyay, Experimental and theoretical investigation of solubility of carbon dioxide in concentrated aqueous solution of 2-amino-2-methyl-1-propanol and piperazine, J. Chem. Thermodyn. 51 (2012) 120–125.
[85] M. Kundu, B.P. Mandal, S.S. Bandyopadhyay, Vapor−liquid equilibrium of CO_2 in aqueous solutions of 2-amino-2-methyl-1-propanol, J. Chem. Eng. Data 48 (2003) 789–796.
[86] D.-J. Seo, W.-H. Hong, Solubilities of carbon dioxide in aqueous mixtures of diethanolamine and 2-amino-2-methyl-1-propanol, J. Chem. Eng. Data 41 (1996) 258–260.
[87] D. Silkenbäumer, B. Rumpf, R.N. Lichtenthaler, Solubility of carbon dioxide in aqueous solutions of 2-amino-2-methyl-1-propanol and *n*-methyldiethanolamine and their mixtures in the temperature range from 313 to 353 K and pressures up to 2.7 MPa, Ind. Eng. Chem. Res. 37 (1998) 3133–3141.
[88] D. Tong, G.C. Maitland, M.J.P. Trusler, P.S. Fennell, Solubility of carbon dioxide in aqueous blends of 2-amino-2-methyl-1-propanol and piperazine, Chem. Eng. Sci. 101 (2013) 851–864.
[89] P. Tontiwachwuthikul, A. Meisen, C.J. Lim, Solubility of carbon dioxide in 2-amino-2-methyl-1-propanol solutions, J. Chem. Eng. Data 36 (1991) 130–133.
[90] F. Bougie, M.C. Iliuta, CO_2 absorption in aqueous piperazine solutions: experimental study and modeling, J. Chem. Eng. Data 56 (2011) 1547–1554.
[91] P.W.J. Derks, H.B.S. Dijkstra, J.A. Hogendoorn, G.F. Versteeg, Solubility of carbon dioxide in aqueous piperazine solutions, AIChE J. 51 (2005) 2311–2327.
[92] R. Dugas, G. Rochelle, Absorption and desorption rates of carbon dioxide with monoethanolamine and piperazine, Energy Procedia 1 (2009) 1163–1169.
[93] V. Ermatchkov, Á.-P.-S. Kamps, D. Speyer, G. Maurer, Solubility of carbon dioxide in aqueous solutions of piperazine in the low gas loading region, J. Chem. Eng. Data 51 (2006) 1788–1796.
[94] S. Kadiwala, A.V. Rayer, A. Henni, High pressure solubility of carbon dioxide (CO2) in aqueous piperazine solutions, Fluid Ph. Equilibria 292 (2010) 20–28.
[95] Á.-P.-S. Kamps, J. Xia, G. Maurer, Solubility of CO_2 in (H_2O+piperazine) and in (H_2O+MDEA+piperazine), AIChE J 49 (2003) 2662–2670.
[96] O.F. Dawodu, A. Meisen, Solubility of carbon dioxide in aqueous mixtures of alkanolamines, J. Chem. Eng. Data 39 (1994) 548–552.
[97] F.-Y. Jou, F.D. Otto, A.E. Mather, Vapor-liquid equilibrium of carbon dioxide in aqueous mixtures of monoethanolamine and methyldiethanolamine, Ind. Eng. Chem. Res. 33 (1994) 2002–2005.
[98] A. Benamor, M.K. Aroua, Modeling of CO2 solubility and carbamate concentration in DEA, MDEA and their mixtures using the Deshmukh-Mather model, Fluid Ph. Equilibria 231 (2005) 150–162.
[99] G. Kumar, T.K. Mondal, M. Kundu, Solubility of CO2 in aqueous blends of (diethanolamine + 2-amino-2-methyl-1-propanol) and (diethanolamine + N-methyldiethanolamine), J. Chem. Eng. Data 57 (2012) 670–680.
[100] M. Kundu, S.S. Bandyopadhyay, Solubility of CO2 in water+diethanolamine+N-methyldiethanolamine, Fluid Ph. Equilibria 248 (2006) 158–167.
[101] M.E. Rebolledo-Libreros, A. Trejo, Gas solubility of CO_2 in aqueous solutions of N-methyldiethanolamine and diethanolamine with 2-amino-2-methyl-1-propanol, Fluid Ph. Equilibria 218 (2004) 261–267.
[102] F. Murrieta-Guevara, M.a.E. Rebolledo-Libreros, A. Romero-Martínez, A. Trejo, Solubility of CO_2 in aqueous mixtures of diethanolamine with methyldiethanolamine and 2-amino-2-methyl-1-propanol, Fluid Ph. Equilibria 150 (1998) 721–729.

[103] R. Mahmoodi, M. Mofarahi, A.A. Izadpanah, M. Afkhamipour, A. Hajizadeh, Experimental and theoretical investigation of equilibrium absorption performance: effect of alkyl amines as promoters on the CO_2 loading of 2-amino-2-methyl-1-propanol at 313 K, Energ. Fuel 33 (2019) 8985–8997.
[104] M. Kundu, S.S. Bandyopadhyay, Solubility of CO2 in water+diethanolamine+2-amino-2-methyl-1-propanol, J. Chem. Eng. Data 51 (2006) 398–405.
[105] M. Shokouhi, A.T. Zoghi, M. Vahidi, B. Moshtari, Solubility of carbon dioxide in aqueous blends of 2-amino-2-methyl-1-propanol and *N*-methyldiethanolamine, J. Chem. Eng. Data 60 (2015) 1250–1258.
[106] H. Suleman, A.S. Maulud, Z. Man, Experimental measurements and modelling of carbon dioxide solubility in aqueous AMP/MDEA and Piperazine/MDEA blends, Fluid Ph. Equilibria 463 (2018) 142–148.
[107] A. Böttger, V. Ermatchkov, G. Maurer, Solubility of carbon dioxide in aqueous solutions of N-methyldiethanolamine and piperazine in the high gas loading region, J. Chem. Eng. Data 54 (2009) 1905–1909.
[108] S.K. Dash, S.S. Bandyopadhyay, Studies on the effect of addition of piperazine and sulfolane into aqueous solution of N-methyldiethanolamine for CO_2 capture and VLE modelling using eNRTL equation, J. Greenh. Gas Control 44 (2016) 227–237.
[109] P. Brúder, A. Grimstvedt, T. Mejdell, H.F. Svendsen, CO_2 capture into aqueous solutions of piperazine activated 2-amino-2-methyl-1-propanol, Chem. Eng. Sci. 66 (2011) 6193–6198.
[110] S.K. Dash, A. Samanta, A. Nath Samanta, S.S. Bandyopadhyay, Absorption of carbon dioxide in piperazine activated concentrated aqueous 2-amino-2-methyl-1-propanol solvent, Chem. Eng. Sci. 66 (2011) 3223–3233.
[111] Z.-Y. Yang, A.N. Soriano, A.R. Caparanga, M.-H. Li, Equilibrium solubility of carbon dioxide in (2-amino-2-methyl-1-propanol+piperazine+water), J. Chem. Thermodyn. 42 (2010) 659–665.
[112] S. Trenn, Multilayer perceptrons: approximation order and necessary number of hidden units, IEEE Trans. Neural Netw. 19 (2008) 836–844.
[113] X. Glorot, Y. Bengio, Understanding the difficulty of training deep feedforward neural networks, in: Proceedings of the Thirteenth International Conference on Artificial Intelligence and Statistics, 2010, pp. 249–256.